Advances in Applied Mathematics and Mechanics
Adv. Appl. Math. Mech., Vol. **6**, No. 2, pp. 233-246

DOI: 10.4208/aamm.12-m1277
April 2014

Analysis of Functionally Graded Piezoelectric Cylinders in a Hygrothermal Environment

M. N. M. Allam[1], A. M. Zenkour[2,3,*] and R. Tantawy[4]

[1] *Department of Mathematics, Faculty of Science, Mansoura University, Mansoura 35516, Egypt*
[2] *Department of Mathematics, Faculty of Science, King Abdulaziz University, P.O. Box 80203, Jeddah 21589, Saudi Arabia*
[3] *Department of Mathematics, Faculty of Science, Kafrelsheikh University, Kafr El-Sheikh 33516, Egypt*
[4] *Department of Mathematics, Faculty of Science, Damietta University, 34517, Egypt*

Received 18 May 2012; Accepted (in revised version) 28 August 2013

Available online 7 April 2014

Abstract. This paper presents an analytical solution for the interaction of electric potentials, electric displacement, elastic deformations, and describes hygrothermal effect responses in hollow and solid cylinders, subjected to mechanical load and electric potential. Exact solutions for displacement, stresses and electric potentials in functionally graded piezoelectric material are determined using the infinitesimal theory. The material properties coefficients of the present cylinder are assumed to be graded in the radial direction by a power law distribution. Numerical examples display the significant of influence of material inhomogeneity. It is interesting to note that selecting a specific value of inhomogeneity parameter can optimize the piezoelectric hollow and solid cylinders responses, which will be of particular importance in modern engineering designs.

AMS subject classifications: 74-XX

Key words: Functionally graded, piezoelectric material, hygrothermal effect.

1 Introduction

Functionally graded materials (FGMs) are microscopically inhomogeneous composite materials, in which the volume fraction of two or more materials is varied smoothly and continuously as a function of position along certain dimension of the structure from one

*Corresponding author.
Email: zenkour@kaf-sci.edu.eg (A. M. Zenkour)

point to other [1]. These materials are mainly constructed to operate in high temperature environments.

The functionally graded piezoelectric material (FGPM) is a kind of piezoelectric material with material composition and properties varying continuously in certain direction. The piezoelectric devices can be entirely made of FGPM or use FGPM as a transit inter layer between two different piezoelectric materials. FGPM is composite material intentionally designed to possess desirable properties for some specific applications. The advantage of this new kind of materials can improve the reliability or the service life of piezoelectric devices.

In view of the advantages of FGMs, a number of investigations dealing with thermal stresses had been published in the scientific literature. In recent years, Tanigawa et al. [2] derived a one-dimensional temperature solution for inhomogeneous plate in transient state and also optimized the material composition by introducing a laminated composite model. Zimmerman and Lutz [3] determined the exact solution of thermal stresses and thermal expansions for a uniformly heated FG cylinder. They derived a governing equation for the thermo-elastic equilibrium of the cylinder, by substituting stress strain and kinematic relations into the stress equilibrium equation of cylinder allowing the elastic moduli and thermal expansion coefficient to vary in the radial direction. Then the equation was solved analytically. The mechanical properties of FGMs are often being represented in the exponentially graded form [4–6] and power-law variations one [1, 7–15]. Reddy [1] analyzed the static behavior of FG rectangular plates based on his third-order shear deformation plate theory. Reddy and Chin [10] studied the dynamic thermoelastic response of FG cylinders and plates. In Reddy and Cheng [11], three-dimensional thermomechanical deformations of simply supported, FG rectangular plates were studied by using an asymptotic method.

A new beam element has been developed to study the thermoelastic behavior of FG beam structures by Chakraborty et al. [16] using the first-order shear deformation theory. Nadeau and Ferrari [17] presented a one dimensional thermal stress analysis of a transversely isotropic layer that was inhomogeneous in its thickness. Using the infinitesimal theory of elasticity, Naki and Murat [18] obtained closed-form solutions for stresses and displacements in FG cylindrical and spherical vessels subjected to internal pressure. Dai et al. [19] presented closed form solutions for a FGM hollow cylinder, closed form solutions for the through thickness stresses and perturbation of the magnetic field vector. Allam and Tantawy [20] present an analytical solution for the interaction of electric potentials, electric displacements, elastic deformations and thermoelasticity, and describes electromagnetoelastic responses and perturbation of the magnetic field vector in hollow structures subjected to mechanical load and electric potential. They consider the solution for the case of hollow structure made of viscoelastic isotropic material, reinforced by elastic isotropic fibers; this material is considered as structurally anisotropic material. More reports on FG structures may also be found in the literature, such as [21–23].

The degradation in performance of the structure due to moisture concentration and high temperature has become increasingly more important with the prolonged use of

FGMs in many structural applications. As a result, hygrothermal internal stresses are generated with the change of environment. These stresses generally induce large deformation and could even contribute to the failure of the structure. The deformation and stresses analysis of different plate structures subjected to moisture and temperature has been the subject of research interest of many investigators [24–28].

This article is concerned with the effects of the graded material profile on the response of piezoelectric cylinders in a hygrothermal environment. The hollow and solid cylinders are subjected to mechanical load and electric potential. Analytical solutions for the interaction of electric potentials, electric displacement, elastic deformations, and describe hygrothermal effect responses, are presented. The infinitesimal theory is used to determine the displacement, stresses and electric potentials in functionally graded piezoelectric cylinders.

2 Formulation of the problem

The present paper is upon employing simplifying assumptions, to present an analytical solution of FGPM hollow and solid cylinders as shown in Fig. 1. The electric displacement, stresses and electric potential in these cylinder will be investigated. Consider a long FGPM cylinder having perfect conductivity. Let the cylindrical coordinates of any representative point be (r,θ,z) and assume that the FGPM cylinder is subjected to a rapid change in temperature $T(r)$ and moisture concentration $C(r)$. For the axisymmetric plane strain assumption, the components of displacement, stresses, and electric displacement and electric potential may be expressed as $u(r)$, $\sigma_i(r)$, $D_r(r)$ and $\psi(r)$, respectively. The constitutive relations are:

$$\begin{Bmatrix} \sigma_r \\ \sigma_\theta \\ \sigma_z \end{Bmatrix} = \begin{bmatrix} c_{rr} & c_{r\theta} & e_{rr} \\ c_{r\theta} & c_{\theta\theta} & e_{r\theta} \\ c_{rz} & c_{\theta z} & e_{rz} \end{bmatrix} \begin{Bmatrix} \dfrac{du}{dr} \\ \dfrac{u}{r} \\ \dfrac{d\psi}{dr} \end{Bmatrix} - \begin{Bmatrix} \lambda_r \\ \lambda_\theta \\ \lambda_z \end{Bmatrix} T(r) - \begin{Bmatrix} \eta_r \\ \eta_\theta \\ \eta_z \end{Bmatrix} C(r) \tag{2.1}$$

and

$$D_r = e_{rr}\frac{du}{dr} + e_{r\theta}\frac{u}{r} - \varepsilon_{rr}\frac{d\psi}{dr} + p_{11}T(r) + p_{22}C(r), \tag{2.2}$$

where c_{ij} $(i=r,\theta,\ j=r,\theta,z)$, e_{rj} $(j=r,\theta,z)$, ε_{rr}, p_{11} and p_{22} are elastic coefficients, piezoelectric parameters, dielectric parameters and pyroelectric coefficients, respectively. In addition, η_i $(i=r,\theta,z)$ are the coefficients of moisture expansion, while λ_i represent the stress-temperature moduli that take the forms

$$\begin{Bmatrix} \lambda_r \\ \lambda_\theta \\ \lambda_z \end{Bmatrix} = \begin{bmatrix} c_{rr} & c_{r\theta} & c_{rz} \\ & c_{\theta\theta} & c_{\theta z} \\ \text{symm.} & & c_{zz} \end{bmatrix} \begin{Bmatrix} \alpha_r \\ \alpha_\theta \\ \alpha_z \end{Bmatrix}, \tag{2.3}$$

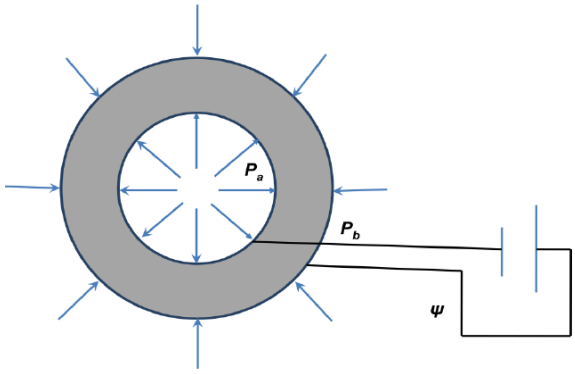

Figure 1: A cross-sector of a functionally graded piezoelectric hollow cylinder.

in which α_i are the thermal expansion coefficients. Generally, this study assumes that c_{ij}, e_{rj}, α_i $(i,j=r,\theta,z)$, ε_{rr}, p_{11} and p_{22} of the FG cylinder change continuously through the radial direction of the cylinder.

The graded between the physical properties and the radial direction r for the present cylinder is given by

$$P=P^0r^\beta, \tag{2.4}$$

where P^0 is the material property of the homogeneous cylinder and β is a geometric parameter. The value β equals zero represents a fully homogeneous cylinder. The above power law assumption reflects variable properties applied only to the radial direction. The power law exponent β may be varied to obtain different distributions of the components materials through the radial direction of the cylinder. The range $-2\leq\beta\leq2$ is used in the present study to cover all values of the coordinate exponent encountered in [5,17]. However, these values of β do not necessarily represent a certain material, various β values are used to demonstrate the effect of inhomogeneity on the electric displacement, stresses and electric potential.

3 Governing equations

3.1 Equation of temperature

The temperature distribution through the radial direction of the cylinder is governed by the heat conduction equation

$$\kappa\nabla^2T(r)+q(r)=0, \tag{3.1}$$

where

$$\nabla^2=\frac{d^2}{dr^2}+\frac{1}{r}\frac{d}{dr},$$

κ is the thermal conductivity and $q(r)$ is the heat generation function.

3.2 Equation of moisture

In modeling, the transient moisture diffusion equation is analogous to the transient heat conduction equation. It can be described by Fick's law as

$$\nabla^2 C(r)=0. \tag{3.2}$$

3.3 Equations of equilibrium

The equilibrium equation of the FGPM cylinder, in the absence of body forces, is expressed as

$$\frac{d\sigma_r}{dr}+\frac{\sigma_r-\sigma_\theta}{r}=0. \tag{3.3}$$

In the absence of free charge density, the charge equation of electrostatics [29] is expressed as

$$\frac{dD_r}{dr}+\frac{D_r}{r}=0. \tag{3.4}$$

4 Solution of the problem

The elastic solutions for the FGPM hollow and solid circular cylinders are given by solving all of temperature, moisture, and equilibrium equations. These solutions are completed by the application of the mechanical, electric, and boundary conditions.

4.1 Elastic solution for the FGPM hollow circular cylinder

The present FGPM hollow circular cylinder is considered with inner radius a and outer radius b. The temperature is generated at a position-dependent rate within the inner surface and it transfers to the outer one, while the outer surface is insulated. The boundary conditions for temperature are

$$T(r)|_{r=a}=T_0, \quad \frac{dT(r)}{dr}\Big|_{r=b}=0, \tag{4.1}$$

where T_0 is the reference initial temperature. The internal energy generation within the inner and outer surface is described by the heat generating function

$$q(r)=\frac{Q}{ab}(r-a)(b-r), \quad a\le r\le b, \tag{4.2}$$

where Q represents the constant rate of internal energy generation. So, the general solution of the heat conduction equation given in Eq. (3.1) is

$$T(r)=\frac{Qr^2}{144\kappa ab}[9(r^2+4ab)-16r(a+b)]+c_1\ln(r)+c_2, \tag{4.3}$$

where c_1 and c_2 are arbitrary integration constants that determined from the boundary conditions, Eqs. (4.1), in the forms:

$$\begin{cases} c_1=\dfrac{Qb^2}{12\kappa a}(b-2a), \\ c_2=\dfrac{Q}{144\kappa ab}[a^3(7a-20b)-12b^3\ln(a)(b-2a)]+T_0. \end{cases} \tag{4.4}$$

Also the general solution of the moisture equation, given in Eq. (3.2) is

$$C(r)=c_3\ln(r)+c_4, \tag{4.5}$$

where c_3 and c_4 are arbitrary integration constants. The boundary conditions for the moisture concentration are

$$C(r)|_{r=a}=0, \quad C(r)|_{r=b}=C_0, \tag{4.6}$$

where C_0 is the reference initial moisture concentration. Then, the constants c_3 and c_4 are given by

$$c_3=\frac{C_0}{\ln(b)-\ln(a)}, \quad c_4=-\frac{C_0\ln(a)}{\ln(b)-\ln(a)}. \tag{4.7}$$

In addition, the solution of the charge equation of electrostatics is given by

$$D_r=\frac{A_1}{r}, \tag{4.8}$$

where A_1 is unknown constant. Thus, Eqs. (2.2) and (4.8) with the aid of the gradation relation, given in Eq. (2.4) give

$$\frac{d\psi}{dr}=\frac{1}{\varepsilon^0_{rr}}\left(e^0_{rr}\frac{du}{dr}+e^0_{r\theta}\frac{u}{r}+p^0_{11}T(r)+p^0_{22}C(r)-\frac{A_1}{r^{\beta+1}}\right). \tag{4.9}$$

The radial and circumference stresses given in Eq. (2.1) with the aid of Eqs. (2.4) and (4.9) can be summarized as

$$\begin{aligned} \begin{Bmatrix} \sigma_r \\ \sigma_\theta \end{Bmatrix} =& r^\beta \left(\begin{bmatrix} m_{11} & m_{12} \\ m_{12} & m_{22} \end{bmatrix} \begin{Bmatrix} \dfrac{du}{dr} \\ \dfrac{u}{r} \end{Bmatrix} - \begin{Bmatrix} \lambda^0_r r^\beta - m_{31} \\ \lambda^0_\theta r^\beta - m_{32} \end{Bmatrix} T(r) - \begin{Bmatrix} m_{41} \\ m_{42} \end{Bmatrix} C(r) \right) \\ & - \begin{Bmatrix} m_{51} \\ m_{52} \end{Bmatrix} \frac{A_1}{r}, \end{aligned} \tag{4.10}$$

where

$$\begin{cases} m_{11}=c^0_{rr}+\dfrac{(e^0_{rr})^2}{\varepsilon^0_{rr}}, & m_{12}=c^0_{r\theta}+\dfrac{e^0_{rr}e^0_{r\theta}}{\varepsilon^0_{rr}}, & m_{22}=c^0_{\theta\theta}+\dfrac{(e^0_{r\theta})^2}{\varepsilon^0_{rr}}, \\ m_{31}=\dfrac{e^0_{rr}p^0_{11}}{\varepsilon^0_{rr}}, & m_{32}=\dfrac{e^0_{r\theta}p^0_{11}}{\varepsilon^0_{rr}}, & m_{41}=\eta^0_r-\dfrac{e^0_{rr}p^0_{22}}{\varepsilon^0_{rr}}, \\ m_{42}=\eta^0_\theta-\dfrac{e^0_{r\theta}p^0_{22}}{\varepsilon^0_{rr}}, & m_{51}=\dfrac{e^0_{rr}}{\varepsilon^0_{rr}}, & m_{52}=\dfrac{e^0_{r\theta}}{\varepsilon^0_{rr}}. \end{cases} \tag{4.11}$$

Therefore, Eq. (3.3) with the aid of Eq. (4.10), yields

$$\frac{d^2u}{dr^2}+\frac{\beta+1}{r}\frac{du}{dr}+\frac{\hat{m}_{12}}{r^2}u=\varphi(r), \tag{4.12}$$

where

$$\begin{aligned}\varphi(r)=&\left(\left[\bar{\lambda}_r^0(2\beta+1)-\bar{\lambda}_\theta^0\right]r^\beta+\hat{m}_{32}\right)\frac{T(r)}{r}+(\bar{\lambda}_r^0 r^\beta-\bar{m}_{31})\frac{dT}{dr}-\hat{m}_{42}\frac{C(r)}{r}\\&+\bar{m}_{41}\frac{dC}{dr}-\frac{\bar{m}_{52}}{r^{\beta+2}}A_1,\end{aligned} \tag{4.13}$$

and

$$\begin{cases}\hat{m}_{12}=\beta\bar{m}_{12}-\bar{m}_{22}, \quad \bar{\xi}=\dfrac{\xi}{m_{11}}, \quad \hat{m}_{32}=\bar{m}_{32}-\bar{m}_{31}(\beta+1),\\ \hat{m}_{42}=\bar{m}_{42}-\bar{m}_{41}(\beta+1).\end{cases} \tag{4.14}$$

The general solution of Eq. (4.12) is given by

$$u=B_1r^{R_1}+B_2r^{R_2}+U_p, \tag{4.15}$$

where B_1 and B_2 are arbitrary integration constants and R_1 and R_2 are the roots of the equation $m^2+\beta m+\hat{m}_{12}=0$. The particular solution U_p is given by

$$U_p=\frac{1}{R_1-R_2}\left[r^{R_1}\int r^{1-R_1}\varphi(r)dr-r^{R_2}\int r^{1-R_2}\varphi(r)dr\right]. \tag{4.16}$$

The constants B_1 and B_2 can be obtained from the mechanical boundary conditions:

$$\sigma_r|_{r=a}=-P_1, \quad \sigma_r|_{r=b}=-P_2, \tag{4.17}$$

where P_1 and P_2 are the inner and outer pressures, respectively. So, the complete general solution to the radial displacement u may be used to obtain the electric potential. Integrating Eq. (4.9) gives the electric potential $\psi(r)$ with additional arbitrary integration constant A_2. Finally, the constants A_1 and A_2 can be given by using the electric boundary conditions:

$$\psi(r)|_{r=a}=\psi_1, \quad \psi(r)|_{r=b}=\psi_2. \tag{4.18}$$

Therefore, the final forms of stresses in the hollow cylinder can be obtained by using Eqs. (4.10) with the aid of Eqs. (4.3), (4.5), and (4.15).

4.2 Elastic solution for the FGPM solid circular cylinder

Let the present FGPM circular cylinder is solid with outer radius a. The temperature is generated at a position-dependent rate within the surface. The boundary conditions for temperature are

$$T(r)|_{r=a}=T_0, \quad \frac{dT(r)}{dr}\Big|_{r=0}=0, \tag{4.19}$$

where T_0 is the reference initial temperature. The internal energy generation is described by the heat generating function

$$q(r)=\frac{Q}{a}(a-r), \quad 0\le r\le a. \tag{4.20}$$

The general solution of the heat conduction equation given in Eq. (3.1) is

$$T(r)=\frac{Qr^2}{36\kappa a}(9a-4r)+\bar{c}_1\ln(r)+\bar{c}_2, \tag{4.21}$$

where $\bar{c}_1$ and $\bar{c}_2$ are arbitrary integration constants that determined from the boundary conditions, Eqs. (4.19), in the forms:

$$\bar{c}_1=\frac{Qa^2}{6\kappa}, \quad \bar{c}_2=\frac{Qa^2}{36\kappa}[5-6\ln(a)]+T_0. \tag{4.22}$$

The boundary conditions for the moisture concentration, in this case, are

$$C(r)|_{r=0}=0, \quad C(r)|_{r=a}=C_0, \tag{4.23}$$

where C_0 is the reference initial moisture concentration. So, the general solution of the moisture equation, given in Eq. (3.2) is

$$C(r)=C_0. \tag{4.24}$$

For solid cylinder, we assume that D_r is vanished and Eq. (2.2) gives,

$$\frac{d\psi}{dr}=\frac{1}{\varepsilon^0_{rr}}\left(e^0_{rr}\frac{du}{dr}+e^0_{r\theta}\frac{u}{r}+p^0_{11}T(r)+p^0_{22}C(r)\right). \tag{4.25}$$

The radial and circumference stresses given in Eq. (2.1) with the aid of Eqs. (2.4) and (4.25) can be summarized as

$$\left\{\begin{array}{c}\sigma_r\\ \sigma_\theta\end{array}\right\}=r^\beta\left(\left[\begin{array}{cc}m_{11} & m_{12}\\ m_{12} & m_{22}\end{array}\right]\left\{\begin{array}{c}\frac{du}{dr}\\ \frac{u}{r}\end{array}\right\}-\left\{\begin{array}{c}\lambda^0_r r^\beta-m_{31}\\ \lambda^0_\theta r^\beta-m_{32}\end{array}\right\}T(r)-\left\{\begin{array}{c}m_{41}\\ m_{42}\end{array}\right\}C(r)\right), \tag{4.26}$$

where m_{ij} are given in Eq. (4.11). Therefore, Eq. (3.3) with the aid of Eq. (4.26), yields

$$\frac{d^2u}{dr^2}+\frac{\beta+1}{r}\frac{du}{dr}+\frac{\hat{m}_{12}}{r^2}u=\bar{\varphi}(r), \tag{4.27}$$

where

$$\bar{\varphi}(r)=\big(\big[\bar{\lambda}_r^0(2\beta+1)-\bar{\lambda}_\theta^0\big]r^\beta+\hat{m}_{32}\big)\frac{T(r)}{r}+(\bar{\lambda}_r^0 r^\beta-\bar{m}_{31})\frac{dT}{dr}$$
$$+\hat{m}_{42}\frac{C(r)}{r}-\bar{m}_{41}\frac{dC}{dr}. \tag{4.28}$$

Similarly, the general solution of Eq. (4.27) is given by

$$u=\bar{B}_1 r^{R_1}+\bar{B}_2 r^{R_2}+\bar{U}_p, \tag{4.29}$$

where $\bar{B}_1$ and $\bar{B}_2$ are arbitrary integration constants and R_1 and R_2 are the roots of the equation $m^2+\beta m+\hat{m}_{12}=0$. The particular solution $\bar{U}_p$ is given as in Eq. (4.16) by replacing $\varphi(r)$ with $\bar{\varphi}(r)$. Also, the constants $\bar{B}_1$ and $\bar{B}_2$ can be obtained from the mechanical boundary conditions:

$$u|_{r=0}=0, \quad \sigma_r|_{r=a}=-P_2. \tag{4.30}$$

So, the complete general solution to the radial displacement u may be used to obtain the electric potential. Integrating Eq. (4.25) gives the electric potential $\psi(r)$ with arbitrary integration constant A which is determined from the electric boundary condition:

$$\psi(r)|_{r=a}=\psi_2. \tag{4.31}$$

Therefore, the final forms of stresses in the solid cylinder can be obtained by using Eqs. (4.26) with the aid of Eqs. (4.21), (4.24) and (4.29).

5 Numerical examples and discussion

Numerical examples for the analysis of FGPM cylinders in a hygrothermal environment will be given. These numerical computations are carried out for the temperature, displacement and stresses that being reported herein are in the dimensionless forms:

$$\bar{r}=\frac{r}{a}, \quad \bar{T}=\frac{T}{T_0}, \quad \bar{C}=\frac{C}{C_0}, \quad \bar{\psi}=\frac{\psi}{10^2\psi_2}, \quad \bar{\sigma}_r=\frac{\sigma_r}{10^2P_2}, \quad \bar{\sigma}_\theta=\frac{\sigma_\theta}{10^3P_2}.$$

Computations were carried out for the following values of parameters:

$c_{rr}^0=1.11\times10^{11}\text{Pa}$, $c_{r\theta}^0=7.78\times10^{10}\text{Pa}$, $c_{rz}^0=1.15\times10^{11}\text{Pa}$,
$c_{\theta\theta}^0=2.2\times10^{11}\text{Pa}$, $e_{rr}^0=15.1\text{c/m}^2$, $e_{r\theta}^0=-5.2\text{c/m}^2$,
$\varepsilon_{rr}^0=5.62\times10^{-5}\text{c}^2/\text{Km}^2$, $p_{11}^0=p_{22}^0=-2.5\times10^{-5}\text{c/Km}^2$,
$\alpha_r^0=\alpha_z^0=0.0001\text{K}^{-1}$, $\alpha_\theta^0=0.00001\text{K}^{-1}$, $\kappa=0.35\text{W/KM}$,
$\eta_r^0=0.06\times c_{rr}^0$, $\eta_\theta^0=0$.

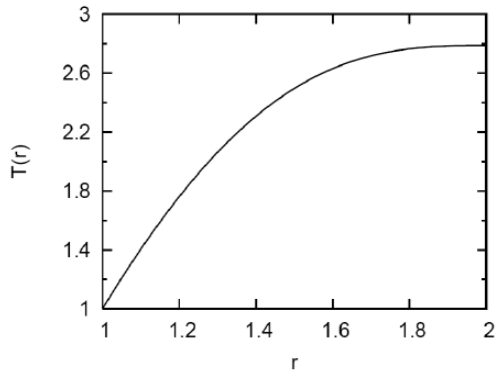

Figure 2: Temperature distribution in the FGPM hollow cylinder.

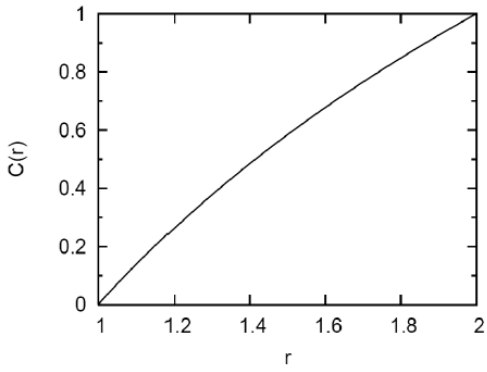

Figure 3: Moisture distribution in the FGPM hollow cylinder.

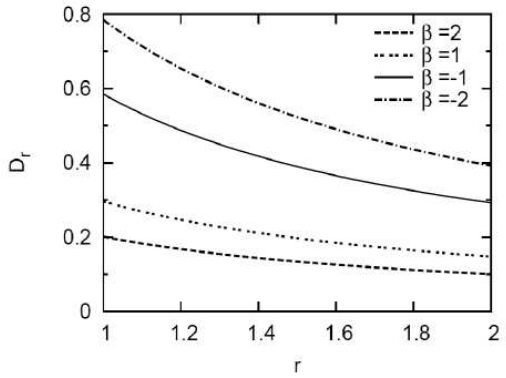

Figure 4: Electric displacement distributions in the FGPM hollow cylinder for different value of β.

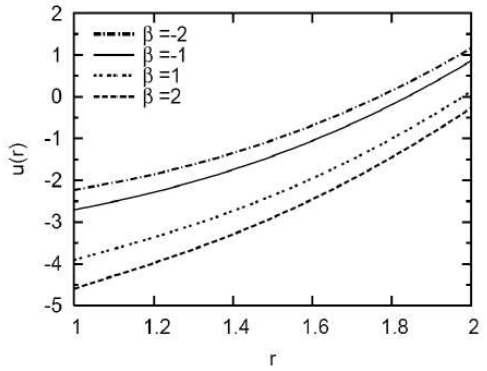

Figure 5: Displacement in the FGPM hollow cylinder for different value of β.

In addition, the following constants for the rate of internal energy Q, the internal P_1 and external P_2 pressures as well as the internal ψ_1 and external ψ_2 electric potentials, are used:

$$Q=12\text{W/m}^3, \quad P_1=0\text{Pa}, \quad P_2=10^7\text{Pa}, \quad \psi_1=0\text{W/A}, \quad \psi_2=100\text{W/A}.$$

For simplicity, the symbol bars are replaced by the original symbol in all figures. Numerical results for the FGPM hollow cylinders ($b=2a$) are plotted in Figs. 2-8. The behaviors of temperature and moisture through the radial direction of the hollow cylinders are illustrated in Figs. 2 and 3. Fig. 4 shows the electric displacement distribution along the radial direction of the FGPM hollow cylinder. Different values of the power exponent β are used. The electric displacement decreases as r increases for different values of β. It is also noted that D_r decreases as β increases and this irrespective of its position. Fig. 5 shows the radial displacement distribution along the radial direction of the FGPM hollow cylinder. The radial displacement increases as r increases and as β decreases. It is to

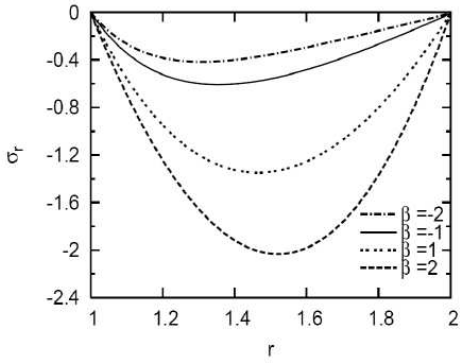

Figure 6: Radial stress distribution in the FGPM hollow cylinder for different value of β.

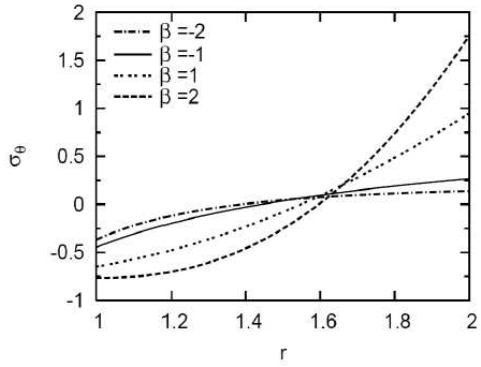

Figure 7: Circumferential stress distribution in the FGPM hollow cylinder for different value of β.

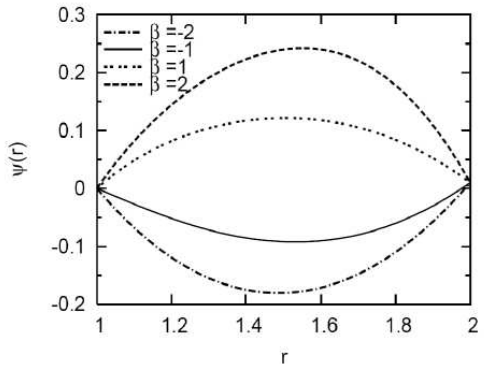

Figure 8: Electric potential distribution in the FGPM hollow cylinder for different value of β.

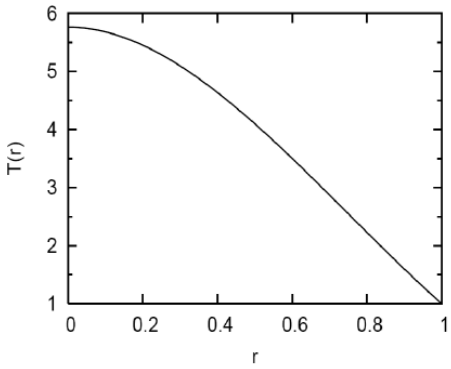

Figure 9: Temperature distribution in the FGPM solid cylinder.

be noted that the radial displacement changes its sign from negative to positive along the radial direction.

The radial σ_r and circumferential σ_θ stresses are plotted in Figs. 6 and 7 along the radial direction of the hollow cylinder. The radial stress σ_r has different minimum points according to the value of β. For negative β, the minimum radial stress occurs near the inner surface of the cylinder while it occurs near the outer surface of the cylinder for positive values of β. It is noticed that the value of β has no effect on σ_θ when $r = 1.615$ at which all circumferential stresses have the same value. On the left hand side of this position σ_θ decreases as β increases and vise versa on the right hand side. The distribution of the electric potential $\psi(r)$ along the radial direction of the hollow cylinder is shown in Fig. 8. The plots of ψ are concave up for positive values of β and concave down for negative values of β.

Once again, the numerical results for the FGPM solid cylinders are plotted in Figs. 9-13. The behavior of temperature through the radial direction of the hollow cylinder is illustrated in Fig. 9. The minimum temperature occurs at the external surface of the solid cylinder. Fig. 10 shows the radial displacement distribution along the radial direction of

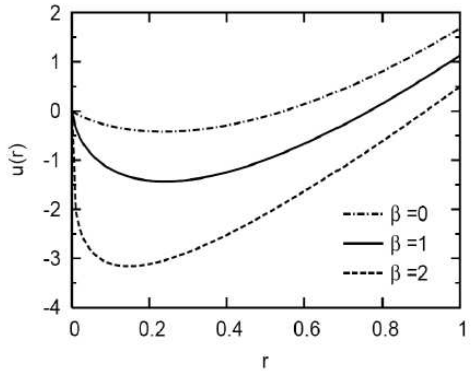

Figure 10: Displacement distribution in the FGPM solid cylinder for different value of β.

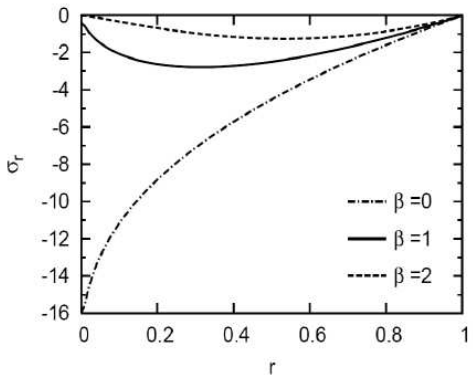

Figure 11: Radial stress distribution in the FGPM solid cylinder for different value of β.

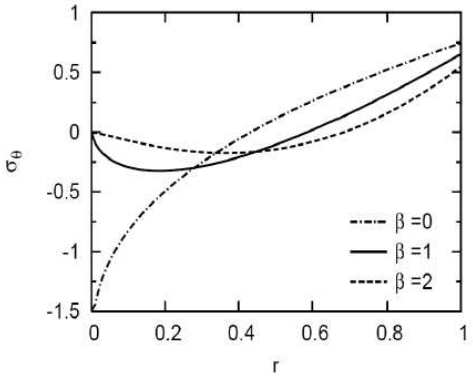

Figure 12: Circumferential stress distribution in the FGPM solid cylinder for different value of β.

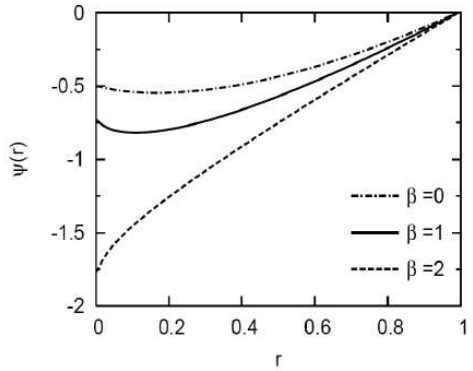

Figure 13: Electric potential distribution in the FGPM hollow cylinder for different value of β.

the FGPM solid cylinder. The radial displacement is no longer increases and has minimum values at $r \cong 0.17, 0.23, 0.25$ for $\beta = 2, 1$, and 0, respectively. The radial σ_r and circumferential σ_θ stresses as well as the electric potential ψ are plotted in Figs. 11-13 along the radial direction of the solid cylinder. All of these components increase directly through the radial direction of the homogeneous solid cylinder $(\beta = 0)$. Other components of stresses and electric potential are no longer increase and have minimum values along the radial direction for $\beta = 1$ and 2. The maximum circumferential stress and electric potential occur at the outer surface of the cylinder.

6 Conclusions

In this paper, the exact solutions for FGPM cylinders having perfect conductivity have been obtained. An analytical solution technique is developed for the electro-thermo-hygro-mechanical problem, where stresses are produced under combined thermome-

chanical and electrical loading conditions. The result of this investigation are validated with the recently published paper [19, 20] with the exception that hygrothermal distribution is also considered in the present study and this might be responsible for little variation which could be noted in stress and electric potential curves produced. The inhomogeneous constants presented in this study are useful parameters from a design point of view. The inhomogeneity parameter is considered as a power-law exponent. However, other types of material inhomogeneity that can be tailored for specific applications to control hygrothermal distribution, stresses and electric potential distribution can be used. Variation of normalized stresses, electric potential and displacement of boundary conditions for different material inhomogeneity parameters β were plotted against dimensionless radius. In general, radial stresses and electrical potentials satisfy the mechanical and electrical boundary conditions at the inner and outer surfaces of the FGPM cylinders.

It is to be shown that the gradient index β has a great effect on the stresses, electric potentials and hygrothermal distribution of the FGPM cylinders. Thus by selecting a proper β value, engineers can design specific FGPM solid and hollow cylinders that can meet some special requirements. In addition, the inclusion of temperature as well as the moisture concentration has a great effect on the behavior of the present cylinders.

It is concluded from the above analyses and discussions that the presented analytical solution is accurate and reliable, and the method is simple and effective. Although the paper considers the case in which the material constants are of power functions in the redial direction, the technique is applicable to other material inhomogeneity.

References

[1] J. N. REDDY, *Analysis of functionally graded plates*, Int. J. Numer. Meth. Eng., 47 (2000), pp. 663–684.

[2] Y. TANIGAWA, M. MATSUMOTO AND T. AKAI, *Optimization of material composition to minimize thermal stresses in non-homogeneous plate subjected to unsteady heat supply*, Jpn. Soc. Mech. Eng. Int. J. Ser. A, 40 (1997), pp. 84–93.

[3] R. W. ZIMMERMAN AND M. P. LUTZ, *Thermal stresses and thermal expansion in a uniformly heated functionally graded cylinder*, J. Thermal Stresses, 22 (1999), pp. 177–188.

[4] B. V. SANKAR, *An elasticity solution for functionally graded beams*, Compos. Sci. Tech., 61 (2001), pp. 689–696.

[5] A. M. ZENKOUR, *Benchmark trigonometric and 3-D elasticity solutions for an exponentially graded thick rectangular plate*, Arch. Appl. Mech., 77 (2007), pp. 197–214.

[6] A. M. ZENKOUR, K. A. ELSIBAI AND D. S. MASHAT, *Elastic and viscoelastic solutions to rotating functionally graded hollow and solid cylinders*, Appl. Math. Mech. Engl. Ed., 29 (2008), pp. 1601–1616.

[7] R. A. ARCINIEGA AND J. N. REDDY, *Large deformation analysis of functionally graded shells*, Int. J. Solids Struct., 44 (2007), pp. 2036–2052.

[8] R. KADOLI, K. AKHTAR AND N. GANESAN, *Static analysis of functionally graded beams using higher order shear deformation theory*, Appl. Math. Model., 32 (2008), pp. 2509–2525.

[9] G. N. PRAVEEN AND J. N. REDDY, *Nonlinear transient thermoelastic analysis of functionally graded ceramic-metal plates*, Int. J. Solids Struct., 35 (1998), pp. 4457–4476.
[10] J. N. REDDY AND C. D. CHIN, *Thermomechanical analysis of functionally graded cylinders and plates*, J. Thermal Stresses, 21 (1998), pp. 593–626.
[11] J. N. REDDY AND Z. Q. CHENG, *Three-dimensional thermomechanical deformations of functionally graded rectangular plates*, Euro. J. Mech. A/Solids, 20 (2001), pp. 841–855.
[12] A. M. ZENKOUR, *A comprehensive analysis of functionally graded sandwich plates: part 1, deflection and stresses*, Int. J. Solids Struct., 42 (2005), pp. 5224–5242.
[13] A. M. ZENKOUR, *A comprehensive analysis of functionally graded sandwich plates: part 2, buckling and free vibration*, Int. J. Solids Struct., 42 (2005), pp. 5243–5258.
[14] A. M. ZENKOUR, *Generalized shear deformation theory for bending analysis of functionally graded plates*, Appl. Math. Model., 30 (2006), pp. 67–84.
[15] A. M. ZENKOUR AND N. A. ALGHAMDI, *Thermoelastic bending analysis of functionally graded sandwich plates*, J. Mater. Sci., 43 (2008), pp. 2574–2589.
[16] A. CHAKRABORTY, S. GOPALAKRISHNAN AND J. N. REDDY, *A new beam finite element for the analysis of functionally graded materials*, Int. J. Mech. Sci., 45 (2003), pp. 519–539.
[17] J. C. NADEAU AND M. FERRARI, *Microstructural optimization of a functionally graded transversely isotropic layer*, Mech. Mater., 31 (1999), pp. 637–651.
[18] T. NAKI AND O. MURAT, *Exact solutions for stresses in functionally graded pressure vessels*, Compos. B, 32 (2001), pp. 683–686.
[19] HONG-LIANG DAI, LI HONG, YI-MING FU AND XIA XIAO, *Analytical solution for electro-magneto-thermo-elastic behaviors of a functionally graded piezoelectric hollow cylinder*, Appl. Math. Model., 34 (2010), pp. 343–357.
[20] M. N. M. ALLAM AND R. TANTAWY, *Thermomagnetic viscoelastic responses in a functionally graded hollow structures*, Acta Mech. Sinica, 27 (2011), pp. 567–577.
[21] M. K. GHOSH AND M. KANORIA, *Analysis of thermoelastic response in a functionally graded spherically isotropic hollow sphere based on Green-Lindsay theory*, Acta Mech., 207 (2009), pp. 51–67.
[22] X. Y. LI, H. J. DING AND W. Q. CHEN, *Axisymmetric elasticity solutions for a uniformly loaded annular plate of transversely isotropic functionally graded materials*, Acta Mech., 196 (2008), pp. 139–159.
[23] S. UEDA, *A cracked functionally graded piezoelectric material strip under transient thermal loading*, Acta Mech., 199 (2008), pp. 53–70.
[24] A. BAHRAMI AND A. NASIER, *Interlaminar hygrothermal stresses in laminated plates*, Int. J. Solids. Struct., 44 (2007), pp. 8119–8142.
[25] A. BENKHEDDA, A. TOUNSI AND E. A. ADDA BEDIA, *Effect of temperature and humidity on transient hygrothermal stresses during moisture desorption in laminated composite plates*, Compos. Struct., 82 (2008), pp. 629–635.
[26] S. H. LO, W. U. ZHEN, Y. K. CHEUNG AND C. WANJI, *Hygrothermal effects on multilayered composite plates using a refined higher order theory*, Compos. Struct., 92 (2010), pp. 633–646.
[27] B. P. PATEL, M. GANAPATHI AND D. P. MAKHECHA, *Hygrothermal effect on the structural behavior of thick composite laminates using higher-order theory*, Compos. Struct., 56 (2002), pp. 25–34.
[28] J. M. WHITENY AND J. E. ASHTON, *Effect of environment on the elastic response of layered composite plates*, AIAA J., 9 (1971), pp. 1708–1713.
[29] P. HEYLIGER, *A note on the static behavior of simply-supported laminated piezoelectric cylinders*, Int. J. Solids Struct., 34 (1996), pp. 3781–3794.